

Multiaxial Deformation and Fatigue Behaviors Under Discriminating Strain Paths

N. Shamsaei¹, A. Fatemi¹, and D. F. Socie²

¹ Mechanical, Industrial and Manufacturing Engineering, The University of Toledo, 2801 West Bancroft Street, Toledo, OH 43606, USA, afatemi@eng.utoledo.edu

² Mechanical Science and Engineering, University of Illinois at Urbana-Champaign, 1206 West Green St., MC-244, Urbana, IL 61801, USA, dsocie@illinois.edu

ABSTRACT. *The effect of incremental and random sequence of variable amplitude axial-torsion straining on stress response and fatigue life of 1050 QT steel with no non-proportional cyclic hardening, and 304L stainless steel with significant non-proportional cyclic hardening were investigated. Predicted stress responses based on a plasticity model using a small number of material parameters are compared with experimental observations and empirical predictions. Observed fatigue behavior under the discriminating strain paths employed is also presented and discussed.*

INTRODUCTION

Service loading or local stress histories of many components and structures are typically multiaxial and variable amplitude rather than constant amplitude. Many multiaxial fatigue models relating multiaxial fatigue life to uniaxial fatigue properties have been developed. Among these, critical plane approaches which reflect damage mechanism within the material have been generally accepted to be more accurate than classical or empirical approaches [1].

Critical plane approaches can be based on only strain, only stress, or both stress and strain. The strain term in models based on both stress and strain is typically the driving damage parameter, while the stress term has a secondary influencing effect. Such strain-stress-based critical plane approaches can also have an energy interpretation, be used for both short and long life fatigue regimes, and can take into account constitutive behavior of the material, such as non-proportional hardening.

Two widely used strain-stress-based critical plane models are the Fatemi-Socie (FS) parameter [2] for shear failure mode materials, and the Smith-Watson-Topper parameters [3] for tensile failure mode materials. Cyclic hardening due to non-proportionality of the loading, as well as mean and/or residual stress effects can also be taken into consideration by the normal stress term in these models [4].

Strain-stress-based critical plane approaches, however, require knowledge of the stress response of the material, either obtained experimentally, or predicted by empirical approaches or constitutive models. Empirical formulations are widely used due to their

simplicity, however, they may result in significant errors when used for general non-proportional loadings [5]. Plasticity or constitutive models are typically based on either Mroz [6] or Armstrong-Frederick [7] multiple surface models. This latter model has been suggested as a proper basis for modeling non-proportional cyclic hardening [8, 9].

Another challenging issue in fatigue life estimation under general variable amplitude multiaxial loading is identification of the loading cycles. There are several proposed methods in the literature for cycle counting under such loading conditions [10-12]. Bannantine and Socie [11] proposed a method based on rainflow cycle counting on candidate critical planes within the material. Based on this method, for shear failure mode materials the shear strain history is rainflow cycle counted as the main channel. The normal stress, as the auxiliary channel, is then determined for each counted shear strain cycle. The counted shear strain and normal stress are used for damage calculation.

In this study, two very different materials in terms of non-proportional hardening were used to investigate cyclic deformation and fatigue behaviors under some discriminating axial-torsion strain paths, using incremental and random sequences of straining. A simplified plasticity model is employed to predict stress response under the aforementioned strain paths. Fatigue lives for the different strain paths used are also compared and damage accumulation on various planes within the material is evaluated.

EXPERIMENTAL PROGRAM

Medium carbon 1050 quenched and tempered (QT) steel and 304L stainless steel (SS) thin-walled tubular specimens were utilized in this study. Monotonic as well as cyclic in-phase and 90° out-of-phase stress-strain curves for the two materials are presented in Fig. 1. As can be seen from this figure, 1050 QT steel is a cyclic softening material and not sensitive to non-proportionality of loading, whereas 304L SS is a cyclic hardening material and exhibits significant additional hardening under 90° out-of-phase loading.

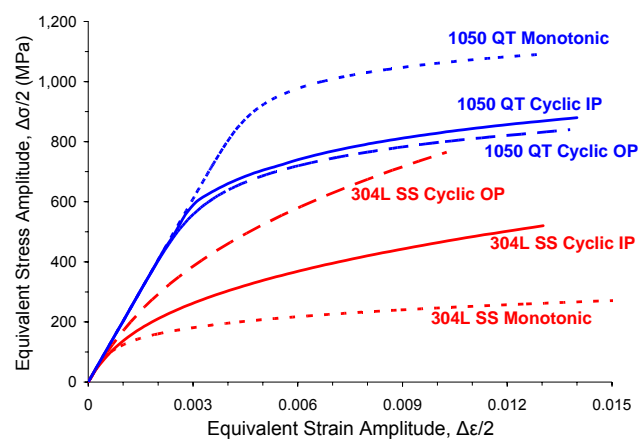


Figure 1 Monotonic, cyclic in-phase (IP), and cyclic 90° out-of-phase (OP) stress-strain curves for 1050 QT steel and 304L stainless steel.

Specimens were designed and fatigue tests were performed according to ASTM Standard E2207 [13] and using a servo-controlled hydraulic axial-torsion load frame. Failure criterion was considered as 5% load or torque drop, whichever occurred first, compared with the stable value obtained at midlife. This load or torque drop corresponded to crack(s) with a length of at least 10 mm on the gage section surface.

In addition to in-phase (IP) and 90° out-of-phase (OP) strain paths, some variable amplitude star shape strain paths, shown in Fig. 2, were utilized for both materials. FRI strain path in Fig. 2 includes 360 proportional fully-reversed axial-torsion cycles with 1° increments starting from the pure axial cycle in $\gamma/\sqrt{3}-\epsilon$ strain space. FRR strain path also includes 360 proportional fully-reversed axial-torsion cycles, but in random sequences in $\gamma/\sqrt{3}-\epsilon$ strain space. This strain path is identical to FRI strain path, except that rather than 1° increment, the sequence of straining is in a random manner between 1° to 360°. The FRI15 strain path is similar to the FRI path, except rather than 1° increments, 15° increments are used (i.e. 24 proportional fully-reversed axial-torsion cycles in a block, rather than 360 cycles). The PI strain path shown in Fig. 2 is also identical to the FRI path, except rather than the fully-reversed cycles for the FRI path (i.e. $R = -1$), the cycles have their minimum at zero for the PI path (i.e. $R = 0$).

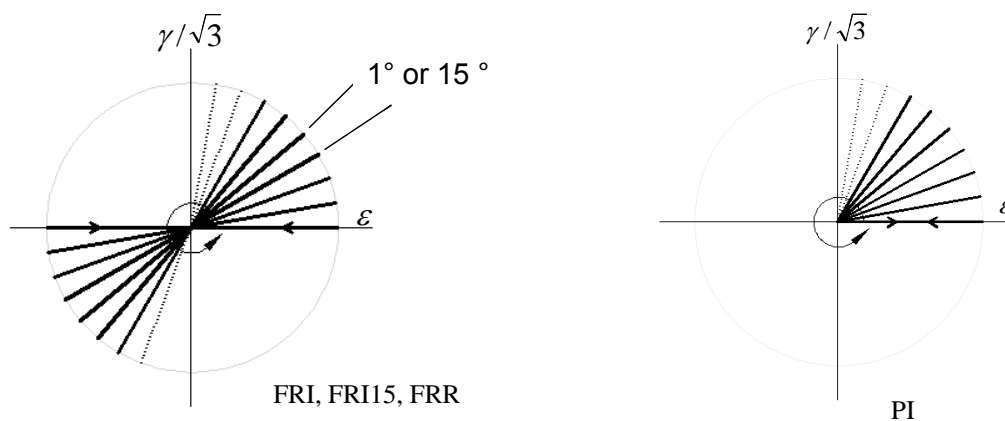


Figure 2 Variable amplitude axial-torsion star shape strain paths utilized.

DEFORMATION BEHAVIOR AND PREDICTIONS

Equivalent stress amplitude response of 1050 QT steel and 304L SS under 0.7% and 0.34% equivalent strain amplitudes for all strain paths used are presented in Fig. 3. Equivalent stress responses in this figure are normalized by the in-phase stress response at the same strain level. Similar results are observed for all strain paths utilized for 1050 QT steel as a material with no non-proportional hardening, whereas significant differences in equivalent stresses are obtained for different strain paths of 304L SS as a material with significant non-proportional cyclic hardening. The FRR strain path with random sequence straining causes severe cross hardening in 304L SS, similar to 90° out-

of-phase loading, resulting in much higher stress than for incremental sequence paths (i.e. IP, FRI and PI).

As the change in straining direction is very slow for FRI strain path (i.e. 1° increments), this strain path activates the slip systems gradually, although in all directions, resulting in much less interaction of slip systems as compared to FRR strain path. Consequently, as can be seen from Fig. 3, the stress response in stainless steel for FRI strain path is only slightly higher than for in-phase loading, and much lower than for FRR strain path. For the FRI15 strain path with 15° incremental change in the straining direction, stress response is between those for FRI and FRR paths, as expected.

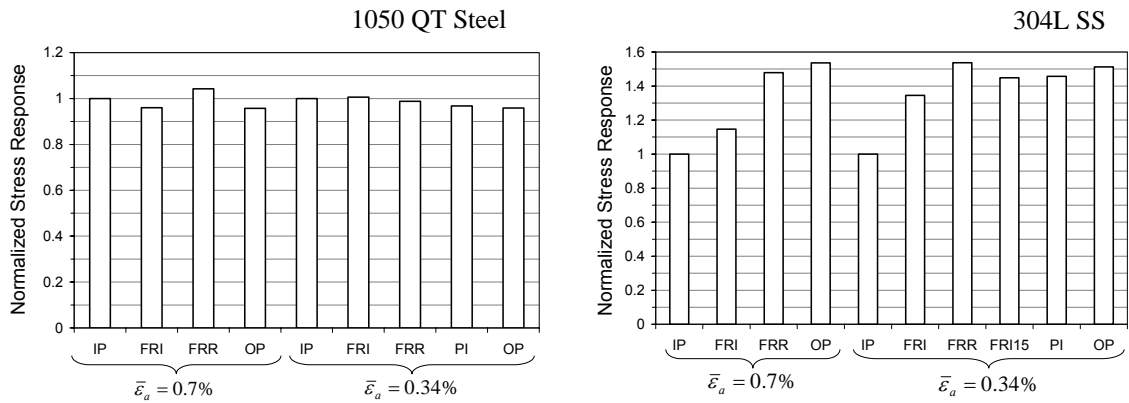


Figure 3 Equivalent stress amplitude responses normalized by the IP data for various strain paths under equivalent strain amplitudes of 0.7% and 0.34%.

Kanazawa et al. empirical formulation [14], which represents the factor of load non-proportionality, F , as the ellipticity of the circumscribed boundary around the strain path in the $\gamma/2$ - ϵ plot, is a commonly used method due to its simplicity. The stress response under non-proportional loading is related to the proportional properties as:

$$\Delta\bar{\sigma}/2 = K'(1 + \alpha F) (\Delta\bar{\epsilon}_p/2)^{n'} \quad (1)$$

where $\Delta\bar{\sigma}/2$ is equivalent stress amplitude, $\Delta\bar{\epsilon}_p/2$ is equivalent plastic strain amplitude, K' is cyclic strength coefficient, n' is cyclic strain hardening exponent, and α is non-proportional cyclic hardening coefficient. Nevertheless, this method cannot distinguish among the star shape strain paths used and predicts the same value of the factor of non-proportionality for all these paths as for the 90° out-of-phase loading since all the paths are within the same circumstantial circle [5].

Armstrong-Frederick [7] incremental plasticity model reflects the strain memory effect and simulates the movement of the yield surface in the deviatoric stress space by a nonlinear kinematic hardening rule. A simplified form of this plasticity model [5] only requiring five material constants (E , G , K' , n' , and α) was used in this study. The non-

proportionality effect in this simplified plasticity model is considered based on Tanaka's non-proportionality parameter [15] as a function of the normalized plastic strain rate vector and the internal microstructure of material, which is represented by a fourth rank tensor in a 5-D plastic strain vector space. The history effects of non-proportional hardening in this model are considered by the evolution equation of an isotropic hardening variable as a function of the non-proportionality parameter.

Comparison of observed and predicted equivalent stress amplitudes based on the simplified plasticity model is presented in Fig. 4 for both materials utilized in this study. As can be seen from this figure, stress responses of variable amplitude multiaxial star shape strain paths are predicted within 12% scatter bands. Therefore, reasonable predictions are obtained by employing Tanaka's non-proportionality parameter coupled with a simplified form of the Armstrong-Frederick incremental plasticity model.

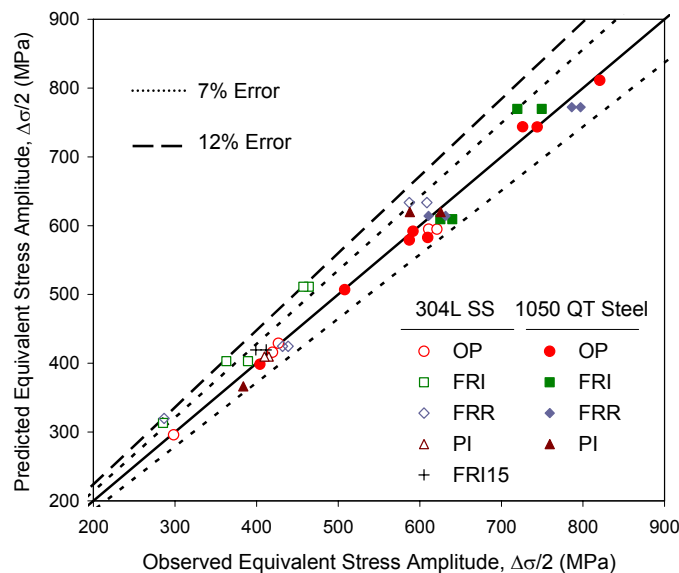


Figure 4 Comparison of observed and predicted equivalent stress amplitudes for 1050 QT steel and 304L SS using a simplified plasticity model [5].

FATIGUE BEHAVIOR

Observed fatigue lives of 1050 QT steel and 304L SS specimens under various star shape strain paths are normalized based on the fatigue life of the in-phase (IP) loading at the same equivalent strain level in Fig. 5. For 1050 QT steel, fatigue lives under FRI and FRR strain paths are about half of the fatigue life under IP (in-phase) strain path at $\bar{\epsilon}_a = 0.7\%$ and about 20% of the IP strain path fatigue life at $\bar{\epsilon}_a = 0.34\%$. The 90° out-of-phase (OP) strain path also results in more than an order of magnitude shorter life, as compared to IP strain path for this material. This is in spite of the fact that the stress response of 1050 QT steel is not sensitive to the non-proportionality of the loading, as

previously discussed (see Fig. 3). Therefore, non-proportional hardening is not the sole reason for the generally observed shorter fatigue lives in non-proportional loading.

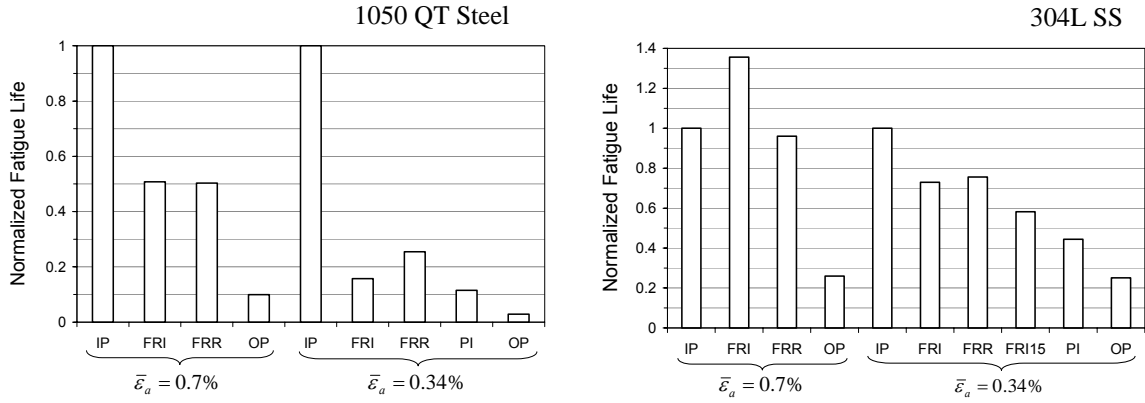


Figure 5 Observed fatigue lives normalized by the IP data for various strain paths under equivalent strain amplitudes of 0.7% and 0.34%.

In the case of 304L SS, the IP, FRR, and FRI strain paths result in comparable fatigue lives at either strain amplitude level, while the 90° out-of-phase (OP) strain path fatigue lives are about 25% of the IP path. Although deformation response of 304L SS is more sensitive to non-proportionality of the loading as compared to the 1050 QT steel, Fig. 5 indicates that fatigue life of 1050 QT steel is more sensitive to loading non-proportionality. Other factors which can explain this behavior are discussed later.

The commonly used von Mises criterion predicts the same fatigue life for IP and OP paths at the same equivalent strain amplitude. Significant difference in fatigue lives observed for these paths for both materials, as observed from Fig. 5, suggests using this criterion results in severe underestimate of fatigue life under non-proportional loading.

Crack orientations for in-phase and 90° out-of-phase paths were observed to coincide with the maximum shear plane with the highest normal stress for both materials, as predicted by the FS parameter. This parameter as a function of maximum shear strain amplitude and maximum normal stress on the maximum shear strain plane, is given as:

$$\frac{\Delta\gamma_{\max}}{2} \left(1 + k \frac{\sigma_{n,\max}}{\sigma_y} \right) = \frac{\tau'_f}{G} (2N_f)^{b_0} + \gamma'_f (2N_f)^{c_0} \quad (2)$$

where σ_y is the yield strength, and τ'_f , b_0 , γ'_f , and c_0 are fatigue properties in the shear form of the strain-life equation. To evaluate damage based on this parameter on each plane and to identify the critical plane as the plane with the greatest value of cumulative damage for star shape strain paths, linear damage rule was used. The plane perpendicular to the specimen longitudinal axis was predicted as the critical plane for all the star shape strain paths. This corresponded to the observed failure plane for each path and for both materials. Details of the analysis and life estimations are reported in [16].

As mentioned earlier, factors other than non-proportional hardening affect fatigue life under non-proportional loading. One such factor is damage distribution, which is generally more widely distributed for non-proportional loading than in proportional loading. Damage distributions for in-phase (IP), 90° out-of-phase (OP), and FRI strain paths are shown in Fig. 6. Damage distributions for other star shape strain paths are similar to that for the FRI strain path. Although the figure shown is for 304L SS, the behavior is similar for the 1050 QT steel. As can be seen, the OP path not only results in the highest damage value, but all planes undergo a significant portion of the maximum damage value. This can explain the significantly shorter life of the OP strain path among all the strain paths. In contrast, for IP strain path only a small number of planes undergo a significant portion of the maximum damage. For the FRI path, although the maximum damage value is lower than for the IP path, all planes undergo a significant portion of the damage. Therefore, accumulation of damage and its distribution on different planes are important considerations in multiaxial fatigue damage analysis.

Another important factor in life estimation is definition of failure. When using crack initiation approaches, failure life is typically defined as the life associated with micro-crack nucleation as well as micro-crack growth on the order of several hundred microns. In experiments, however, fatigue life is typically defined as a crack length corresponding to a certain load drop or stiffness loss. Such cracks are typically longer than several hundred microns in length. Depending on the material fracture toughness, the discrepancy between the two definitions may be small or large. The 304L SS used in this study has higher fracture toughness than the 1050 QT steel. As a result, many micro-cracks were observed on the surface of the 304L SS specimens for all the strain paths investigated. In addition, while many such micro-cracks were present during a significant portion of the fatigue life for 304L SS, they were much smaller in number and appeared much later in life for the 1050 QT steel. This can also explain some of the differences between the observed fatigue lives of the two materials.

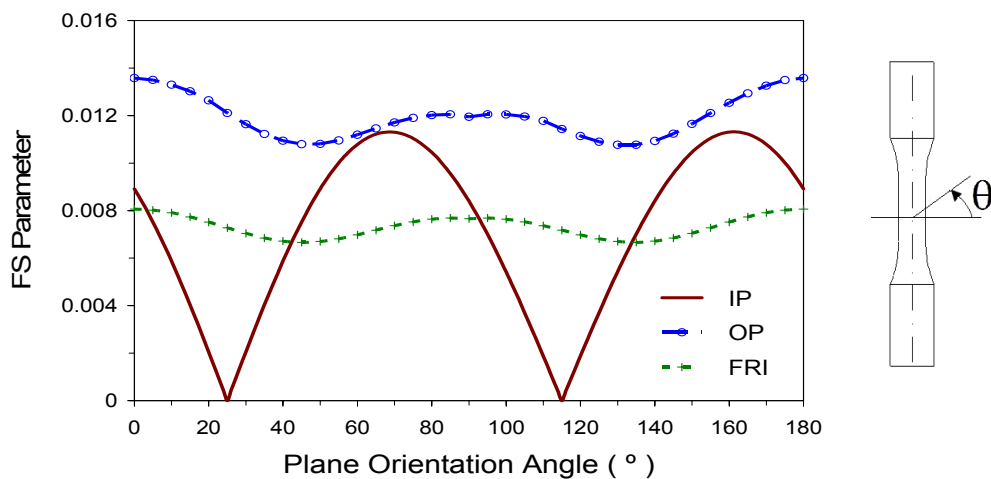


Figure 6 Variation of damage parameter with plane orientation for IP, OP, and FRI strain paths of 304L SS at equivalent strain amplitude of 0.7%.

SUMMARY

The effects of load sequence on deformation and fatigue of 1050 QT steel and 304L SS with different non-proportional hardening characteristics were investigated using discriminating strain paths. The star shape strain path with random straining sequence resulted in significant strain hardening of the 304L SS, as compared to incremental straining sequence. While Kanazawa et al.'s empirical formulation could not distinguish between strain paths with straining in incremental and random manners, stress responses could be predicted well by Tanaka's non-proportionality parameter coupled with a simplified form of the Armstrong-Frederick plasticity model.

In spite of the fact that 1050 QT steel stress response was not sensitive to the non-proportionality of the loading, fatigue life of this material under 90° out-of-phase loading was an order of magnitude shorter than in-phase loading. In addition, fatigue life of 1050 QT steel was more sensitive to loading non-proportionality, compared to 304L SS. Non-proportional hardening is not the sole reason for the generally observed shorter fatigue lives in non-proportional loading. Other factors including the variation of damage distribution on different planes and the extent to which micro-cracks form and grow before causing stiffness loss can also significantly affect fatigue behavior.

REFERENCE

1. Socie, D.F. and Marquis, G.B. (2000) *Multiaxial Fatigue*. SAE Inc.
2. Fatemi, A. and Socie, D.F. (1988) *Fatigue Fract. Eng. Mater. Struct.* **11**: 149-165.
3. Smith, R.N., Watson, P.P., and Topper, T.H. (1970) *J. Mater.* **5**: 767-778.
4. Fatemi, A. and Kurath, P. (1988) *J. Eng. Mater. Tech., Trans. ASME* **110**: 380-388.
5. Shamsaei, N., Fatemi, A., and Socie, D.F. (2010) *Int. J. Plast.* To appear.
6. Mroz, Z. (1969) *Acta Mech.* **7**: 199-212.
7. Armstrong, P.J. and Frederick, C.O. (1966). *Report RD/B/N 731, Central Electricity Generating Board.*
8. Jiang, Y.Y., Kurath, P. (1996) *Int. J. Plast.* **12**: 387-415.
9. Chaboche, J.L. (2008) *Int. J. Plast.* **24**: 1642-1693.
10. ASME boiler and pressure vessel code, Section III, Div. 1, Subsection NB, Class 1 Components, ASME, New York, 1986.
11. Bannantine, J.A. and Socie, D.F. (1991). In: K. Kussmaul, D. McDiarmid, D. Socie (Eds.), *European Structural Integrity Society*, ESIS 10, MEP, London, 35-51.
12. Wang, C.H. and Brown, M.W. (1996) *J. Eng. Mater. Tech., Trans. ASME* **118**: 367-370.
13. ASTM Standard E2207-02 (2007). *Annual Book of ASTM Standards*, ASTM, Vol. 03.01.
14. Kanazawa, K., Miller, K.J., and Brown, M.W. (1979) *Fatigue Eng. Mater. Struct.* **2**: 217-228.
15. Tanaka, E. (1994) *Eur. J. Mech. A. Solids.* **13**: 155-173.
16. Shamsaei, N., Fatemi, A., and Socie, D.F. (2010). Submitted to *Int. J. Fatigue*.